JOURNAL OF APPLIED ELECTROCHEMISTRY 20 (1990) 893–900

Material properties and processing in the production of fuel cell components: I. Hydrogen anodes from Raney nickel for lightweight alkaline fuel cells

W. JENSEIT, A. KHALIL, H. WENDT

Institut für Chemische Technologie der TH Darmstadt, Petersenstrasse 20, 6100 Darmstadt, F.R.G.

Received 12 July 1989; revised 20 December 1989

The production steps of Raney nickel based, PTFE bonded hydrogen anodes for alkaline fuel cells are examined. The Raney nickel catalyst has been made by leaching the nickel aluminium alloy and additional stabilization. The electrode is fabricated by mixing the catalyst with copper oxide for enhancing electronic conductivity and aqueous PTFE emulsion as a hydrophobic binder. Each process step, starting from the nickel aluminium alloy is described and the physical properties of catalyst and electrode are evaluated. At an overpotential of 100 mV the optimized hydrogen anode exhibits at negligable excess hydrogen pressure (1·02 bars) a current density of nearly 400 mA cm^{-2} at 80°C in 30 wt% KOH. Long term performance test shows that electrode overpotential of more than 60 mV should be avoided. A life time of 5000 hrs at 50° C and a current density of 100 mA cm^{-2} has been proven.

1. Introduction

The production of fuel cell electrodes is still more of an art than a scientifically well founded process. This does not reflect the real knowledge of fuel cell producers but rather their understandable interest in maintaining secrecy and to avoid uncontrolled competition. But this policy tends not only to keep the number of competitors small but also limits the market for fuel cell application. The present authors have investigated published or patented procedures for the production of fuel cell components and in this paper we publish our results openly in order to make this information available to potential makers and users of such electrodes.

The guide-line for our research on fuel cell electrodes is the practical or model-based optimisation of the three-fold structural hierarchy of gas consuming porous electrodes. The primary (chemical) structure is the active electrode surface, which determines its electrocatalytic properties, the secondary structure is mainly determined by the fine-porosity. (d_p = 1–10 nm) constituting the inner surface of the catalyst or its support (such as, carbon). The tertiary structure is the intermeshed dual system of coarser pores (d_p > 5 μm) between the catalyst particles, one part of which is hydrophobic and conducts the gases into the fuel cell electrode supplying the electrolyte-wetted catalyst particles with gas, whereas the second, hydrophilic pore system containing the electrolyte enables the passage of ionic current towards the counter electrode.

The first paper in this series deals with hydrogen anodes for alkaline fuel cells prepared from Raney nickel. Such electrodes are usually supported by a nickel screen onto which a felt – a composite made of PTFE-bonded Raney nickel grains – is pressed (Fig. 1).

2. Raney nickel

2.1. *The precursor alloy*

As the precursor of Raney nickel, pulverised aluminium–nickel alloys are usually chosen; these are leached with 30 wt % KOH in order to remove aluminium and to create a highly porous nickel sponge. Figure 2 depicts the main pattern of the binary phase diagram of aluminium and nickel in order to show that the phases Al_3Ni (nearly 50 wt % Ni) and Ni_2Al_3 are clearly distinguished as stoichiometric compounds of considerable stability. Figure 3 shows an X-ray diffractogram of commercially available precursor alloy (DEGUSSA AG), which shows that this Ni–Al alloy consists of the phases $NiAl_3$ and Ni_2Al_3. No NiAl can be detected. The precursor alloys are delivered in pulverized form, the smallest particles measuring approximately 5 μm in diameter, the largest diameters not exceeding 150 μm. This powder was screened and separated into two fractions:

1. particles between 20 and 50 μm
2. particles below 20 μm.

All particles with d_p > 50 μm were discarded. Caustic leaching of the material with 30 wt % KOH as performed in our laboratory, beginning at ambient temperature and ending at 90° C and removing 90–95% of the aluminium from the alloy.

0021-891X/90 $03.00 + .12

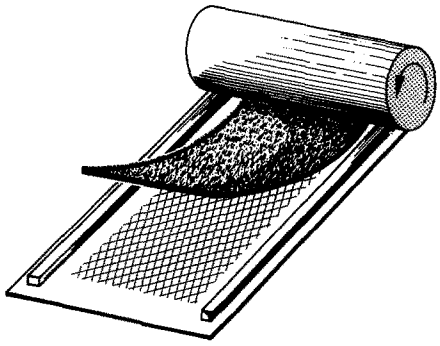

Fig. 1. Schematic of the last fabrication step. The felt is rolled into the net.

2.2. *Leaching of the precursor and stabilisation of the Raney nickel catalyst*

The metallic grains shrink during leaching. A statistical evaluation of the granulometry of the metallic particles before and after leaching shows that their volume loss amounts, on average, to 40% of the initial volume, so that a remarkable fraction of the volume initially occupied by aluminium atoms is lost due to (though incomplete) recrystallisation of the metal. Some earlier investigators (for example, Freel and co-workers [1, 2]) confirm this finding. It is well known that the degree of recrystallisation accompanying leaching is related to the lattice energy of the respective metal (hard metals shrink but little, soft ones like silver or copper are reordered to a larger extent).

The freshly leached Raney nickel contains in its porous structure large amounts of adsorbed hydrogen (approximately 1 atom of hydrogen per 1 atom of nickel exposed to the electrolyte which fills the pores). The X-ray diffractograms of freshly leached Raney nickel shows relatively broad diffraction signals, no NiO and no nickel hydride or any other hexagonal phase (Fig. 4), which had been reported to be produced by the leaching process.

The adsorbed hydrogen causes the pyrophorous reactivity of freshly prepared Raney nickel and has to be removed by slow and controlled oxidation before further processing the material.

The hydrogen loaded catalyst was carefully dried *in vacuo* and the adsorbed hydrogen was catalytically combusted to water by allowing air to slowly enter the vacuum vessel with careful controlling of the flow rate of the air to keep the temperature of the catalyst below

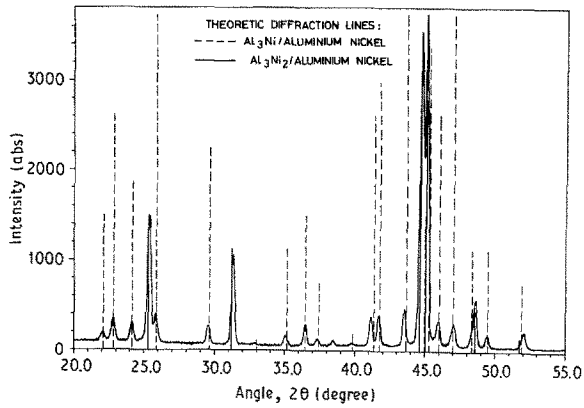

Fig. 3. X-ray diffractogram of the nickel–aluminium alloy, used as precursor for the Raney-nickel electrodes.

100° C. This prevents oxidation of all the nickel and results in oxidation of the surface of the pores only.

Depyrophorisation by reaction with aqueous iodate solution was also investigated [3] by us, although this was not a safe method and frequently resulted in the catalyst igniting spontaneously on exposure to air after oxidation with iodate.

As shown in Fig. 5a the X-ray diffractograms of the oxidized catalyst indicates the presence of nickel oxide and nickel. Both phases are still disordered to some extent as seen from the relatively broad reflection signals.

Annealing of the catalyst in dry nitrogen at 400° C – according to [4] – stabilizes the porous metal by increasing the degree of ordering. The X-ray diffractograms of the annealed catalyst (Fig. 5b) shows narrow signals for Ni as well as for NiO, due to an extension of the coherent ordered areas of the porous material. Chemical analysis of the stabilized catalyst gives 79.5 Ni, 4.5% Al the rest (16 wt %) being oxygen. Therefore nearly half of the nickel must be oxidized to NiO in the annealed catalyst.

2.3. *Granulometry of the catalyst*

As indicated above, the precursor alloy was separated into two fractions: the first fraction comprises crystallites with mean diameters between 50 and 20 μm. The second fraction of the ground-material consists of particles with mean diameters below 20 μm, most of the precursor grains measuring between 10 and 5 μm.

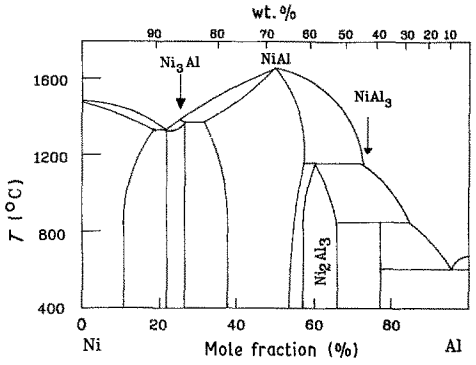

Fig. 2. Phase diagram of the system nickel–aluminium.

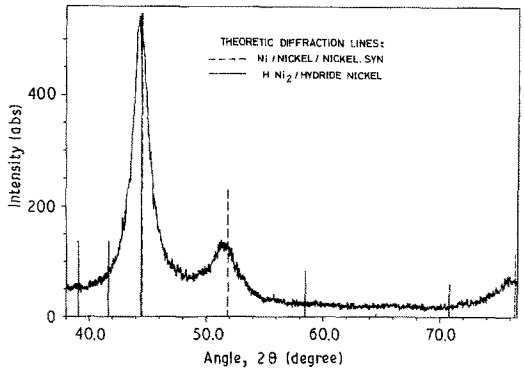

Fig. 4. X-ray diffractogram of freshly leached Raney-nickel.

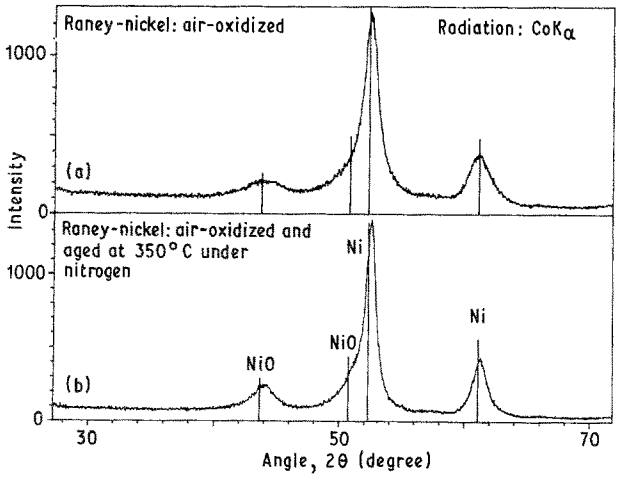

Fig. 5. X-ray diffractogram of: (a) the air oxidized Raney-nickel: (b) the heat conditioned catalyst.

The granulometry of the sieve fraction $d_p < 50\,\mu m$ changes remarkably due to fracturing of the particles during the described treatment consisting of the three steps: (1) caustic leaching (2) depyrophorisation and (3) thermal stabilisation.

Figure 6a depicts a microscopy cross section of the coarse catalyst powder (obtained from sieve-fraction $20\,\mu m < d_p < 50\,\mu m$) being embedded in an organic polymer whereas Fig. 6b shows a picture of the PTFE bounded catalyst (fraction $d_p < 20\,\mu m$) as it consistutes the electrode structure. The coarse catalyst particles (Fig. 6a) maintain their size during leaching although they are divided by cracks and fissures resulting from the strong forces which act on the material during leaching and shrinking.

By contrast, the grains of the precursor alloy with sizes measuring less than $20\,\mu m$ decompose to smaller grains of a mean particle diameter between 3 and $5\,\mu m$ with a very small number of larger grains. Electrodes fabricated from coarser catalyst grains are expected to exhibit lower performance due to mass transfer limitations by slow hydrogen diffusion into the catalyst particles. As was pointed out by Mund [5], Raney-Nickel particles measuring less than $2\,\mu m$ are nearly fully utilized in fuel cell anodes.

2.4. *Measurement of the internal surface of the catalyst*

The leached catalyst was thoroughly washed with distilled water in order to remove all caustic potash. Without subjecting it to depyrophorisation and thermal stabilisation it was transferred to an apparatus for gravimetric BET-determination. After thorough drying *in vacuo* (10^{-4} torr) at room temperature for 12 h, BET-measurements were performed with nitrogen at the temperature of boiling nitrogen.

Figure 7 shows the dependence of adsorbed nitrogen on reduced nitrogen pressure ($P_{red} = P/P^0$, $P^0 = 1$ bar) for the catalyst.

According to the procedure given by Brunauer *et al.* [6] one obtains from this measurement an internal surface of typically $54 \pm 4\,m^2\,g^{-1}$.

3. The PTFE-binder

Polytetrafluorethylene serves as a binder providing cohesion between the catalyst particles and firm

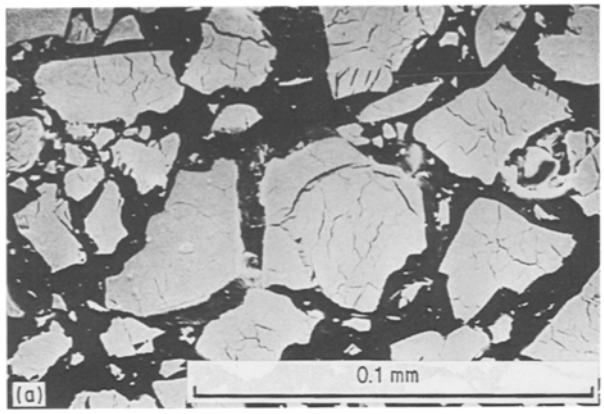

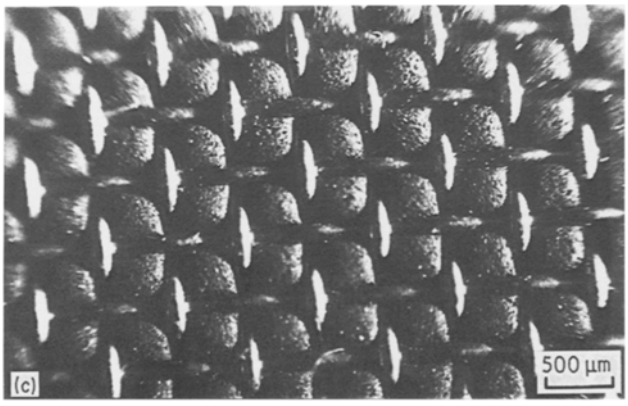

Fig. 6. SEM photograph of: (a) cross-section of the leached, coarse grains dp 750 nm of Raney-nickel catalyst; (b) the PTFE-bonded Raney-nickel; and (c) the reverse of a nickel net supported electrode. Mesh size = 0.5 mm.

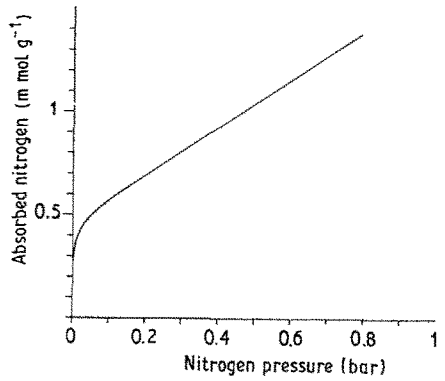

Fig. 7. BET-isotherm of freshly leached Raney-nickel, microporosity of 16 μl g^{-1}, 12%.

mechanical contact of the catalyst with the supporting metal screen. PTFE simultaneously provides the hydrophobic material for the gas-conducting pore system.

PTFE may be supplied either as a powder or as an aqueous emulsion. We have used an aqueous emulsion, which is commercially available (Hostaflon TF 5032) from Hoechst AG. This comes as a 50 wt % mixture stabilized by added polyether. The PTFE-particles are stated to be globular with a mean particle diameter of 0.3 μm.

4. The copper-cement

According to Jung and co-workers [7] impregnating PTFE-bonded porous Raney-nickel hydrogen anodes with metallic copper, enhances the electronic conductivity of the electrode and reduces the voltage drop in the electrode to an extent which allows the anodic current densities to increase threefold without oxidation of the Raney-nickel particles. Copper can be deposited from soluble amine-complexes or by cathodic reduction of solid Cu_2O added to Raney-nickel/PTFE mixtures. The authors have chosen the addition of Cu_2O (Merck p.A. quality) with a mean particle diameter of 30 μm, since it is an easily applied procedure.

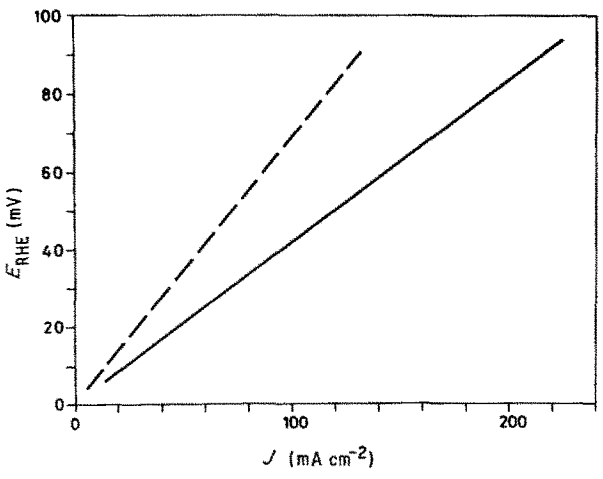

Fig. 8. Potential against current density of Raney-nickel electrodes made after the 'wet' (full line) and 'dry' (dashed line) fabrication method resp., 30% KOH, T = 60° C, $P(H_2)$ = 1.02 bar.

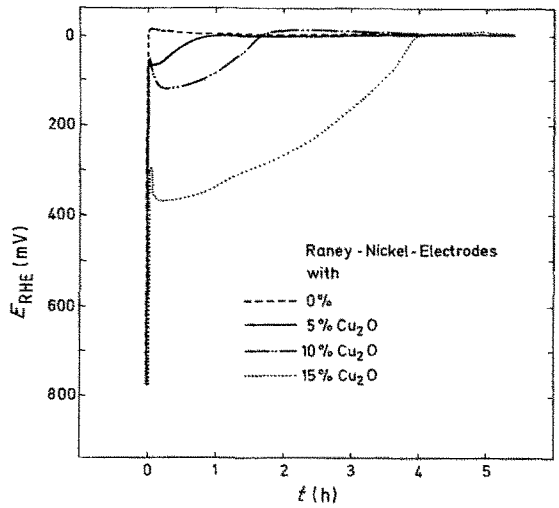

Fig. 9. Potential against time behaviour during cathodic conditioning of electrodes with different copper content. j = 5 mA cm^{-2}, $P(H_2)$ = 1.02 bar, T = 50° C, 30 wt % KOH.

5. The nickel net

Usually nickel nets are used as metallic support for hydrogen anodes of alkaline fuel cells since at the potential of the hydrogen anode nickel is immune to corrosion. Since the thickness of the PTFE bonded Raney-nickel felt for the hydrogen anodes should not exceed 0.5 mm, the mesh width of the net and diameters of the nickel wire had to be of the same or comparable size. Without optimisation of the wire diameter and mesh width* the authors have chosen a net made of nickel wire of 0.2 mm diameter having a mesh width of 0.5 mm.

6. Process steps of hydrogen anode production

6.1. *'Wet' procedure*

6.1.1. Plastic catalyst/PTFE mixtures. The depyrophorized and thermally stabilized catalyst is thoroughly

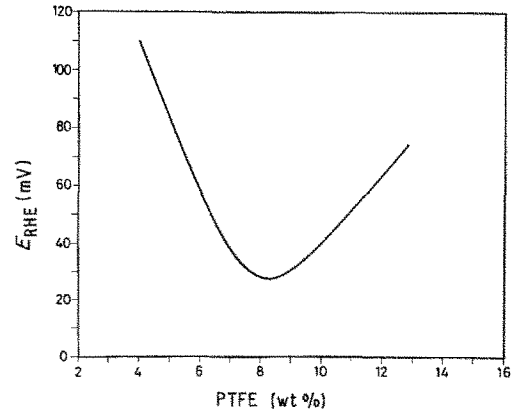

Fig. 10. Polarisation of electrodes with different PTFE content. j = 80 mA cm^{-2}, 30 wt % KOH, T = 80° C, $P(H_2)$ = 1.02 bar.

* The aim of this investigation was mainly to correlate material properties of the consituents of the porous electrode matrix and the relevant properties of the matrix with electrode performance without optimisation of the nickel net.

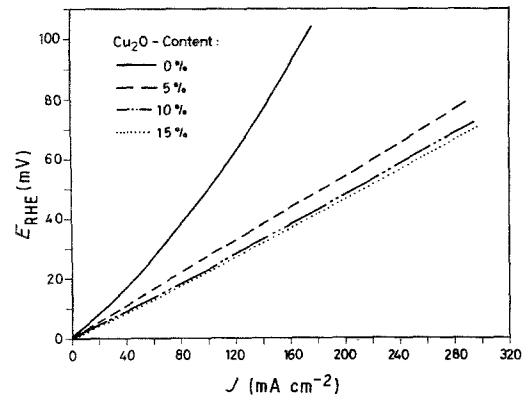

Fig. 11. Polarisation of electrodes with different copper loadings. $P(H_2)$ = 1.02 bar, 30 wt % KOH, T = 80° C, 8 wt % PTFE.

mixed in quantities of 5–10 g with different amounts of Cu_2O in a mortar.

The mixture is added to the appropriate amount of aqueous PTFE-emulsion to obtain the intended PTFE/catalyst ratio. Isopropanol, added to the PTFE-emulsion in 2.5 : 1 weight ratio, stabilized the rubber-like mixture of PTFE, catalyst and Cu_2O which precipitates by mixing the mixture of Raney-nickel and cuprous oxide with the PTFE-emulsion. This mixture still contains a certain amount of water which evaporates slowly together with isopropanol during the following process steps. Isopropanol with a boiling point of 82.3° C, evaporates only slowly and, since it wets PTFE and the catalyst equally well, mediates the stabilisation of the finely dipersed mixtures of the hydrophobic PTFE and hydrophilic catalyst in a plastizisable mass.

6.1.2. Working the PTFE/catalyst into felts and electrodes. Neither bonding between the tiny PTFE-particles and the catalyst nor the mutual bonding of the catalyst by PTFE-fibres is achieved by simply precipitating the plastic mixture. If the mixture is dried, a powder is formed which cannot be worked into a felt by rolling. Cold-rolling the moist mass, however, simultaneously accompanied by the evaporation of water and isopropanol, results in crosslinking of the catalyst particles by PTFE-fibres which is

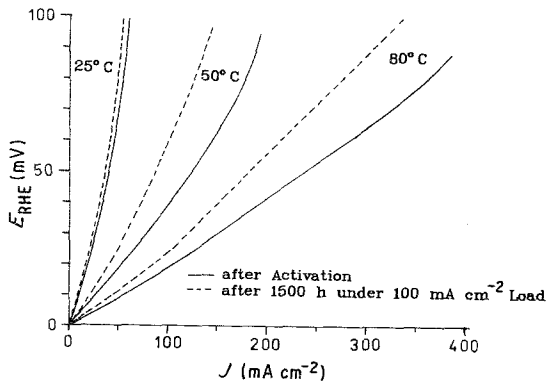

Fig. 12. Potential against current density of hydrogen anode. $P(H_2)$ = 1.02 bar, 30 wt % KOH, (full line) immediately after activation, (dashed line) the same electrode after 1500 h at a load of 100 mA cm^{-2} at 50° C.

obviously brought about (see Fig. 6b) by stress and friction from the initially globular PTFE-particles. This rolling procedure is currently being performed by experience with a 'familiarity for material properties'; it is certainly the least understood and controlled step and still requiring intensive scientific elucidation.

Whilst still wet and containing isopropanol the material is first worked into a felt of 0.5 mm thickness, and then 0.2 mm thickness, and finally is rolled into the nickel net. The electrode preparation is finished by removal of the surfactant, which initially stabilized the PTFE-emulsion. Repeated washing of the electrode with boiling acetone removes the polyether. Omission of this cleaning of the electrode usually results in the electrode being too hydrophilic, hence giving a very poor performance.

Figure 6c demonstrates the 'upper' side of the electrode which is exposed to the gas. The opposite side facing the electrolyte shows nothing in particular and is smoother than the catalyst at the gas side since the roller acts from this side when the felt is pressed into the nickel screen.

With 10 g of PTFE-bonded catalyst approximately 100 cm^2 of anode area can be prepared. Scaling the described procedures for larger (industrial) quantities remains a problem to be solved.

6.2. *Dry procedure*

Intensive blade-milling of a mixture of catalyst and PTFE-powder produces a fluffy mass in which the catalyst and PTFE cannot be distinguished from each other any longer.* This fluffy mixture can be worked into a felt by cold rolling. A comparison of the effective catalystic activity of hydrogen anodes made by the wet and the dry procedure shows quite convincingly that in our case anodes made by the wet procedure (Fig. 8), have a higher effective catalytic activity. The dry mixture demands much higher rolling pressure and strain than the wet procedure. High rolling pressure and stress are supposed to induce a layered structure of the electrode – and in particular alignment of the PTFE-fibres – parallel to the electrode surface. This may increase the diaphragm resistance [8] of the electrode and, additionally, may build up a diffusion barrier for the gases entering (H_2) and leaving (H_2O-vapour) the electrode.

7. Preconditioning of hydrogen anodes

The freshly prepared electrodes cannot be used without an additional cathodic conditioning. This serves to reduce the added Cu_2O with the formation of a metallic, highly conductive copper deposit within the fuel cell electrodes. This is a process composed of two steps: Cu_2O disproportionates and Cu^{2+} is dissolved in the electrolyte being immediately deposited cathodically as copper metal. In this way a homo-

* According to Schnurnberger and co-workers [10] high-speed blade milling of catalyst particles with PTFE leads to PTFE-coatings of the catalyst grains.

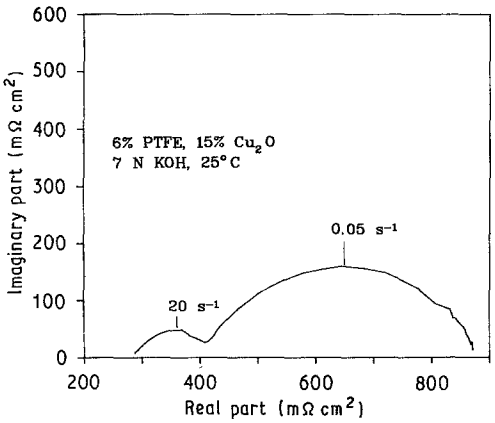

Fig. 13. Nyquist-plot of a hydrogen anode, $E = +10$ mV with respect to RHE, 7 N KOH, $T = 25°C$, $P(H_2) = 1.02$ bar.

geneous deposition of copper in the electrode matrix is achieved, which then has a dark red appearance. This cathodic treatment leads additionally to partial reduction of the nickel oxide.

Figure 8 depicts the variation of the electrode potential during reductive conditioning. The reduction is performed with a cathodic current density of 5 mA cm^{-2} (referred to the geometric surface of the electrode), the electrode being fully immersed in 30 wt % KOH at 50° C.

The different traces in Fig. 9, for electrodes with different Cu_2O contents of 5, 10, 15 wt % (with respect to the catalyst content of the anode), show that the reduction of Cu_2O proceeds at potentials distinctively more positive than the reversible hydrogen electrode (*RHE*). After some time the reduction of Cu_2O is completed and the electrode reaction switches to hydrogen evolution.

According to Bianchi and Longhi the equilibrium potential of the couple Cu_2O/Cu should be +450 mV with respect to *RHE*, which is observed for electrodes containing 15 wt % Cu_2O at the beginning of the cathodic conditioning [9].

BET-measurements of conditioned anodes show a somewhat enhanced surface of the reduced catalyst (84 m^2 g^{-1}) compared to the freshly leached catalyst.

8. Optimisation of the composition of the anode

8.1. *PTFE content*

Apart from a comparison of coarse catalyst powders ($d_p > 50\,\mu$m) with powders of finer granulometry, the optimal contents of Cu_2O, that is, the amount of copper improving the electronic conductivity of the electrode, and of PTFE, determining the percentage of the hydrophobic part of the void of the porous electrode matrix, was determined experimentally by measuring the effect of these parameters on electrode performance.

Figure 10 demonstrates the influence of different amounts of PTFE (in wt % relative to stabilized and oxidized Raney nickel) on the current voltage curves by plotting the anodic overpotential measured at an anodic current density of 80 mA cm^{-2} at 80° C in 30 wt % KOH with respect to the PTFE content. There is a pronounced minimum in the overpotential which implies optimal electrode performance at 8 wt % PTFE.

Table 1. Analysis of impedance spectrum

Polarisation	*Resistance**	*Value* ($\Omega\,cm^2$)
Diaphragm resistance	r_D	0.16
Charge-transfer	r_1	0.04
Hydrogen transfer	r_2	0.26
OH^-/H_2O transfer	h_1	0.12
Double-layer capacity	c_1	0.4 F cm^{-2}

* Symbols according to Fig. 14b.

8.2. *Copper content*

Figure 11 depicts the important effect of improving the internal electronic conductivity of the electrode by impregnation with metallic copper. The slope of the current voltage curve is significantly changed by addition of only 5% Cu_2O reducing the effective electrode resistance by a factor of two. Any further addition of copper up to 15 wt % gives only a slight improvement.

9. Electrode characterisation

9.1. *Temperature dependence of current voltage curves*

In Fig. 12 the current voltage curves are plotted for three different temperatures using hydrogen anodes of optimized composition and structure ($d_p = 3$–$5\,\mu$m – Raney nickel load 90–100 mg cm^{-2}, PTFE: 8 wt % and Cu_2O: 15 wt %). The temperature effect is very pronounced. It is still to be determined whether this is brought about by several different, but partially cooperative and partially counteractive effects for instance, a change in electrolyte/gas holdup of the electrolyte, improvement of electrolyte conductivity, which increases from 25° C to 80° C by more than a factor of 2.5, or whether the increased exchange current density for hydrogen oxidation (change by approximately an order of magnitude) is mainly responsible for the observed effect.

9.2. *Impedance spectroscopy*

A hint at the contributions of Ohmic, Faradaic and mass transport resistances to the effective impedance of the electrode is obtained by impedance measurements. Figure 13 depicts a typical impedance spectrogram of an optimized hydrogen anode, measured at 25° C in the form of Nyquist plot. The low temperature was chosen as at lower temperatures the different

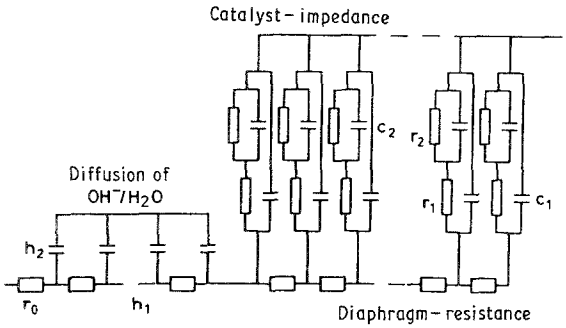

Fig. 14. Electrode impedance according to Mund [10]. r_0 electrolyte resistance; r_1 charge transfer resistance; c_1 double layer capacity; r_2, c_2 hydrogen transport in the pores; h_1, h_2 OH^-/H_2O transport out of the electrode; r_D diaphragm resistance: electrolyte resistance in the electrode structure.

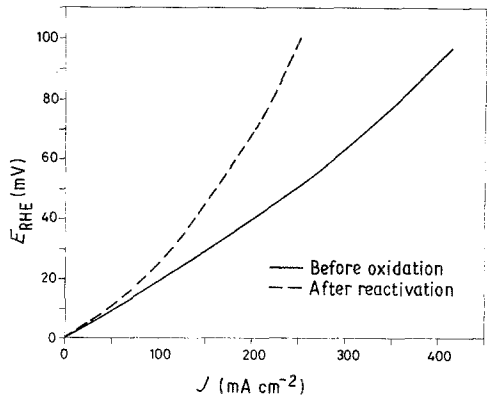

Fig. 16. Potential against current density of freshly activated and reactivated hydrogen anode. $P(H_2)$ = 1.02 bar, T = 80° C, 30 wt % KOH.

impedance contributions are easier to identify than at higher temperatures. Two circles, or near-circles, can be distinguished: one with its apex at 20 Hz is attributed to the electrolyte resistance and effective double layer capacitance of the electrode, whereas the cycle at low frequencies (maximum at approximately 0.05 Hz) may be attributed to an impedance due to diffusive hydrogen transport in the pores and the transport of hydroxide ions out of the electrode. Table 1 summarizes the impedance components obtained by parameter optimisation of the impedance model which is depicted in Fig. 14*.

9.3. *Long-term performance investigations*

The longevity of fuel cell components is of the utmost importance. Therefore a systematic investigation of the life time of Raney-nickel based optimized hydrogen anodes was performed. Figure 15 depicts the change of the electrode potential with time of the anodes (100 mg cm^{-2} Raney nickel, 15 wt % Cu_2O and 8 wt % PTFE) observed under current loads which vary from 100 mA cm^{-2} to 400 mA cm^{-2} and at temperatures across a temperature range from 50° C to 80° C. The electrodes were supplied with hydrogen at 1.02 bar (20 cm hydraulic head). Obviously an anodic current load of 400 mA cm^{-2} at 80° C is too high and at the established anodic overpotential of approximately + 80 mV nickel is unstable and corrodes from the very beginning of the experiment. The anode deteriorates and does not survive for more than 24 h.

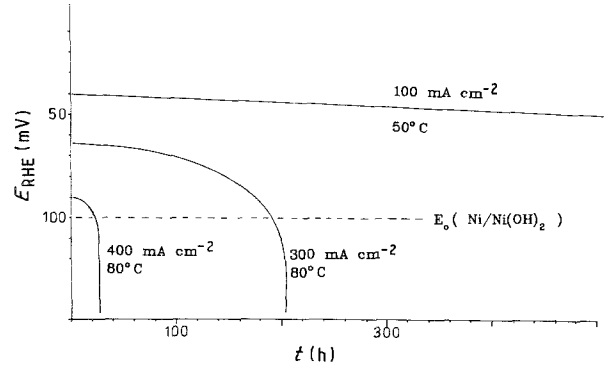

Fig. 15. Potential against time behaviour at different current loads. $P(H_2)$ = 1.02 bar, 30% KOH.

* It should be stressed that at higher temperatures the diagnostic use of impedance spectroscopy is not as clear.

Reduction of the current density to 300 mA cm^{-2} allows the anode to survive for a longer time. But, although an overpotential of + 65 mV at the beginning of the experiment should keep the nickel anode stable, there is a sizeable deterioration observed after only 100 h of operation. It is not unlikely that due to uneven current density and potential distributions and due to hydrogen starvation of minor fractions of the electrode the Raney nickel begins slowly to corrode. This process accelerates remarkably after 150 h so that after 200 h the electrode is destroyed.

Quite different is the behaviour of the electrode at 50° C if it is loaded with a current density of only 100 mA cm^{-2}. Although there is still a slow deterioration detectable which amounts to a rate of 10 μV h^{-1}, one can predict a lifetime of approximately 5000 h, if one expects a final and limiting overpotential of + 70 mV to be critical for approaching an avalanche breakdown of the overpotential. This type of deterioration demonstrates an inherent weakness of Raney-nickel anodes. This effect is overemphasized because of the applied negligible hydrogen overpressure. At 2 bars of hydrogen (1 has the excess) the anodes survive at 80°C and 400 mA cm^{-2} for more than 7000 hrs.

9.4. *Reactivation of spoiled electrodes*

If an anodic overpotential of more than + 300 mV with respect to *RHE* had been safely avoided, oxidized electrodes can be reactivated to a certain extent. Below this overpotential the impregnated copper is still in the metallic state and allows an electronic contact within the electrode. This is an important precondition for reducing oxidized Raney nickel particles. If an anodic overpotential of more than 300 mV is reached then the copper is anodically dissolved and reduction is no longer possible.

Figure 16 compares the anodic current voltage curves of an intact and a revitalized — formerly anodically oxidized — copper impregnated Raney

nickel anode. Revitalisation was accomplished with a cathodic current density of 5 mA cm^{-2} for 5 h at 50° C. Revitalisation is only possible to a limited extent allowing for only half of the initially obtained current density at a given overpotential. Taking into account that in a fully assembled fuel cell the revitalisation procedure would imply an anodic load on the counter electrode – that is, the oxygen cathode, which would be destroyed – it is very unlikely that revitalisation would ever be applied in practice.

10. Conclusion

The preparation of hydrogen anodes for alkaline fuel cells from catalyst powder and aqueous PTFE-emulsions gives a higher electrode activity than the dry procedure using blade milling of PTFE together with the catalyst. The catalyst activity of Raney nickel powders is improved by oxidation under controlled access of air and final thermal annealing. Catalyst grains should, on average, not measure more than 5 μm in diameter. The H_2-anode performance is significantly improved by impregnation of the anode with metallic copper as proposed by Jung *et al.* [7]. A load of approximately 90–100 mg of Raney nickel per cm^2 of electrode surface with approximately 8–9 wt % PTFE and 15 wt % copper gives optimal performance.

Evaluation of the impedance measurements at 25° C after Mund [11] gives a diaphragm resistance of 0.16 Ω cm^2 and a double-layer capacitance of approximately 0.4 F cm^{-2}. With a BET surface of 5.1 m^2 cm^{-2} the converted double-layer capacitance of 8 μF cm^{-2} is somewhat lower than the result of Berndt [12], who has measured 10 μF cm^{-2} at sintered nickel-electrodes, therefore it can be assumed that the electrode is nearly fully utilized. Long term performance is not yet well developed. The authors will report in another paper of this series on means and methods to improve this most important property.

Acknowledgement

The authors are indebted to Kernforschungszentrum Karlsruhe for financially contributing to this investigation and also to the Fonds der Chemischen Industrie and to the Max Buchner Forschungsstiftung for financial support for some of the equipment used.

References

[1] J. Freel, W. J. M. Pieters and R. B Anderson, *J. Catal.* **14** (1969) 247.
[2] *Idem, ibid.* **16** (1970) 281.
[3] H. Ewe, Habilitations-Schrift, Braunschweig, FRG (1974).
[4] A. Winsel, *Dechema Monographs* **98** (1984) 181.
[5] H. Mund, *Siemens Forsch.-u. Entwickl.-Ber.* **4** (1975) 1.
[6] Brunauer, Emmet and Teller, *J. Amer. Chem. Soc.* **60** (1938) 309.
[7] M. Jung and H. v. Döhren, DBP 1 258 398 (1968).
[8] B. Köhler and A. Winsel, *Z. Naturforsch.* **19a** (1964) 602.
[9] G. Bianchi and P. Longhi, *Corros. Sci.* **13** (1973) 853.
[10] K. Bolvin, E. Gulzov and W. Schnurnberger in Fuel Cell Seminar Abstract, Long Beach, Calif. (1988) 164.
[11] H. Mund, *Siemens Forsch.-u. Entwickl.-Ber.* **4** (1975) 68.
[12] D. Berndt, *Electrochim. Acta* **10** (1965) 1067.